

Article

Effect of Si_3N_4 Addition on Oxidation Resistance of ZrB_2 -SiC Composites

Manab Mallik¹, Kalyan Kumar Ray² and Rahul Mitra^{2,*}

¹ Department of Metallurgical and Materials Engineering, National Institute of Technology Durgapur, West Bengal 713209, India; manabmallik@gmail.com

² Department of Metallurgical and Materials Engineering, Indian Institute of Technology Kharagpur, Bengal 713209, India; kkrmt@metal.iitkgp.ernet.in

* Correspondence: rahul@metal.iitkgp.ernet.in; Tel.: +91-322-228-3292

Received: 2 June 2017; Accepted: 26 June 2017; Published: 30 June 2017

Abstract: The oxidation behavior of ZrB_2 -20 vol % SiC and ZrB_2 -20 vol % SiC-5 vol % Si_3N_4 composites prepared by hot-pressing and subjected to isothermal exposure at 1200 or 1300 °C for durations of 24 or 100 h in air, as well as cyclic exposure at 1300 °C for 24 h, have been investigated. The oxidation resistance of the ZrB_2 -20 vol % SiC composite has been found to improve by around 20%–25% with addition of 5 vol % Si_3N_4 during isothermal or cyclic exposures at 1200 or 1300 °C. This improvement in oxidation resistance has been attributed to the formation of higher amounts of SiO_2 and $\text{Si}_2\text{N}_2\text{O}$, as well as a greater amount of continuity in the oxide scale, because these phases assist in closing the pores and lower the severity of cracking by exhibiting self-healing type behavior. For both the composites, the mass changes are found to be higher during cyclic exposure at 1300 °C by about 2 times compared to that under isothermal conditions.

Keywords: borides; ultra-high temperature ceramic composites; oxidation; isothermal; cyclic; residual stress

1. Introduction

Zirconium diboride is considered as one of the most important materials within the ultra-high temperature ceramic (UHTC) group due to its high melting temperature, low theoretical density, high thermal conductivity, good thermal shock resistance and suitable strength at high temperatures [1]. But structural applications of the monolithic ZrB_2 at high temperatures are limited due to its inferior oxidation resistance [2]. Existing literature indicates that reinforcement of ZrB_2 with SiC [2,3] or MoSi_2 [4] or Si_3N_4 [3,5] can lead to improvement in its oxidation resistance and mechanical properties [2–5]. In general, improvement of oxidation resistance of ZrB_2 by the above reinforcements is due to the formation of borosilicate (B_2O_3 - SiO_2) rich scale [2–7]. In addition, improvement of oxidation resistance by addition of SiC in ZrB_2 is associated with improvement in strength and fracture toughness of monolithic ZrB_2 [7]. In an earlier work by the authors, the oxidation behaviors of ZrB_2 -20 vol % SiC and HfB_2 -20 vol % SiC composites were compared, and the results showed that HfB_2 -20 vol % SiC composite possesses superior oxidation resistance compared to that of the ZrB_2 -20 vol % SiC composite. Therefore, an attempt has been made to improve the oxidation resistance of ZrB_2 -20 vol % SiC composite by addition of Si_3N_4 . It has been shown that the addition of 2.5 wt % Si_3N_4 to ZrB_2 significantly aides in its densification [8]. The combined effect of both SiC and Si_3N_4 as reinforcements on the oxidation behavior of ZrB_2 needs further study. For suitable comparison, it is necessary to use some data from our earlier work [6]. This report aims to fill this gap by examining the influence of Si_3N_4 addition on the oxidation behavior of ZrB_2 -SiC composites.

2. Materials and Methods

The mixing of composites having compositions of ZrB₂-20 vol % SiC (ZS) and ZrB₂-20 vol % SiC-5 vol % Si₃N₄ (ZSS) containing raw materials with >99% purity was carried out in acetone medium using vials and balls made of WC-Co composite in a planetary mono-mill (Fritsch GmbH, Idar-Oberstein, Germany) operated at a speed of 250 rpm for 2 h. After the completion of milling, acetone was drained out, and the blended powders were dried at 350 °C for 2 h in air. The composite powders were next crushed using agate mortar and pestle, and then sintered under a uniaxial pressure of 30 MPa using graphite dies lined with grafoil inside a resistance heating furnace operated at 2000 °C for 30 min in an argon environment, to prepare pellets of 42 mm diameter and 4 mm thickness [9].

Sample blanks from the sintered composites with a theoretical density of >99% were characterized by standard metallographic examinations, as well as by X-ray diffraction (XRD) analyses. Isothermal oxidation tests were carried out using samples with dimensions of 4 × 4 × 10 mm³ at 1200 or 1300 °C in a vertical quartz tube furnace for 24 and 100 h in air. The mass of each sample was recorded at intervals of either 1 h (for 24 h tests) or 6 h (for 100 h tests) during isothermal oxidation. In addition, cyclic oxidation studies were carried out on the composites at 1300 °C for a total duration of 24 h in air. The experimental set-up and the method of specimen preparation for isothermal and cyclic oxidation studies have been described in an earlier report [6].

Microstructures of hot-pressed as well as oxidized samples were examined using a field-emission scanning electron microscope (FESEM) equipped with an energy-dispersive spectroscopy (EDS) facility. The cross-sections of the oxidized samples were hot-mounted using copper-resin powder mixture, and were metallographically polished for microstructural examination using a FESEM and electron-probe microanalyzer (EPMA) equipped with wavelength dispersive spectroscopy (WDS) facility. Ten different locations were selected to estimate the averaged oxide scale thicknesses. The grain size, microcrack density and SiO₂ area fractions were measured using images obtained from FESEM with the help of an image analyzer. The biaxial residual stress components in the selected phases of the oxide scales were measured by XRD analysis using the $\sin^2 \psi$ technique [10–12]. The peaks of monoclinic ZrO₂ ($\bar{1}11$) were considered for this measurement. A rocking technique involving tilting of the sample was employed, and the d -spacing (d_ψ) was measured for different angles (ψ) between the surface normal and the normal to the diffracting (hkl) plane. The biaxial stress components in a given phase were calculated from the slopes of the best-fit lines for the plot of d_ψ against $\sin^2 \psi$.

3. Results and Discussion

Figure 1a,b show SEM images depicting the typical microstructures of ZS and ZSS composites, which confirm that there is a uniform distribution of reinforcements. The results for mechanical property evaluation as reported in an earlier publication and summarized in Table 1 have shown that the addition of 5 vol % Si₃N₄ leads to an increase in hardness by 9.3%, flexural strength by 46%, and fracture toughness (obtained by testing of single edge notch-bend tests) by 34.5% [13]. Moreover, the values of Young's modulus are found to be reasonably close to those predicted by the rule of mixtures. These observations of improvement in mechanical properties with the addition of Si₃N₄ can be considered a strong source of motivation for further investigation of the response of these materials to isothermal and cyclic oxidation behavior at elevated temperatures. In an earlier study, Monteverde and Bellosi have examined the mechanical properties and oxidation behavior of ZrB₂-SiC composite hot-pressed at 1870 or 1760 °C using 5 or 3.7 vol % Si₃N₄ as sintering aid as well as Al₂O₃ and Y₂O₃ as additives [14]. The hardness and fracture toughness of the ZSS composites as shown in Table 2 appear to be greater than those (14.6 Hv and 4.55 MPa \sqrt{m}) reported by Monteverde and Bellosi for two composites with similar compositions by 32.5% and 41.6%, respectively. However, the flexural strength found for the ZSS appears to be lower by 40.3%, which could be attributed to finer matrix grain size of the samples investigated by Monteverde and Bellosi [14].

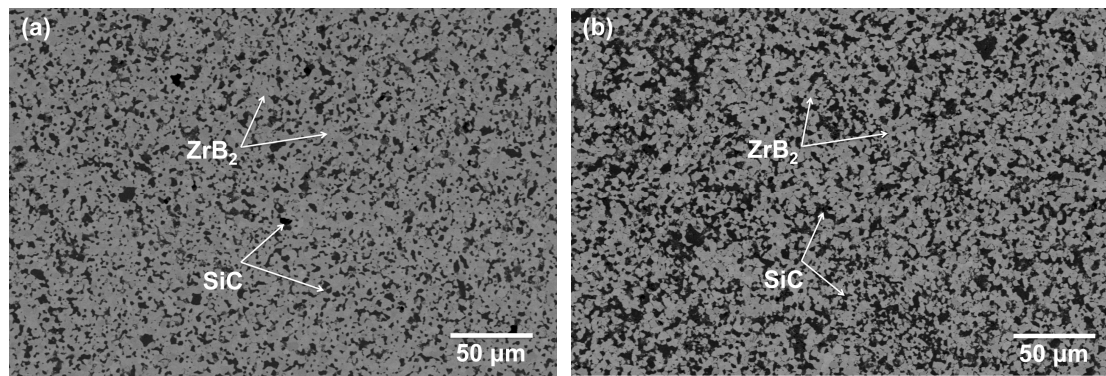


Figure 1. SEM images depicting the microstructures of (a) ZS and (b) ZSS.

Table 1. Room temperature mechanical properties of ZS and ZSS.

Material	Young's Modulus (GPa)	* ROM Young's Modulus (GPa)	Hardness (GPa)	Flexural Strength (MPa)	Fracture Toughness (MPa \sqrt{m})
ZS	484 \pm 3	489	19.4 \pm 0.3	356 \pm 4	5.8 \pm 0.2
ZSS	467 \pm 4	478	21.2 \pm 0.2	520 \pm 6	7.8 \pm 0.6

* The abbreviation "ROM" stands for "Rule of Mixtures" [13].

Table 2. Biaxial principal residual stresses, σ_1 and σ_2 , and maximum residual shear stress, τ_{max} , present in the selected phases of oxide scales of ZS and ZSS subjected to cyclic oxidation at 1300 °C. Values of stress calculated from Equation (5) are also shown for comparison.

Composites	Phase and Plane (<i>hkl</i>)	σ_1 (MPa)	σ_2 (MPa)	τ_{max} (MPa)	Calculated Stress (MPa)
ZSS	ZrO ₂ (−111)	215.8	380.7	−82.45	1700
ZS	ZrO ₂ (−111)	459.2	−5.8	232.5	1700

Figure 2a shows the results of isothermal oxidation tests carried out on the investigated ZrB₂-based composites at 1200 and 1300 °C for 100 h. Oxidation rates (variation of mass-gain per unit area with time) of ZS (at 1200 and 1300 °C) and ZSS (at 1200 °C) composites are found to be almost identical during the first 12 h of exposure; whereas the mass-gain of the ZSS at 1300 °C is lower for the same duration. The oxidation rates are found to decrease with time for both composites with occasional gradual or sharp jumps. The gradual rise in mass-gain after a stable regime may be ascribed to the formation of pores or small cracks, allowing the ingress of oxygen towards the oxide-composite interface. However, occasional sharp increases in mass-gain are considered to be due to cracking and spallation of the oxide scale after growth to a limited thickness. The rate of oxidation of the ZSS is found to be lower than that of the ZS composite at both 1200 and 1300 °C. This observation is in excellent agreement with that of Monteverde and Bellosi, who also reported much lower mass-gain in case of the ZrB₂-20 vol % SiC-5 vol % Si₃N₄ composite compared to that of ZrB₂-5 vol % Si₃N₄ composite [14]. The results of cyclic oxidation tests carried out at 1300 °C for ZS and ZSS composites are also included in Figure 2b. The cyclic oxidation plots are similar in nature for both the composites, and as expected, the ZSS shows lower mass gain compared to that of the ZS composite. Comparison of the results of cyclic and isothermal oxidation tests indicates that: (i) the mass increases during isothermal oxidation in steps; (ii) mass increases or decreases during cyclic exposures more or less continuously, with no apparent regime of zero mass change unlike that observed in the course of isothermal exposure; and (iii) mass changes due to the cyclic oxidation are higher compared to that observed during the isothermal oxidation for both the composites at a given time interval.

Both ZS and ZSS composites exhibit higher mass gain at 1200 °C than that at 1300 °C. Higher mass gain at 1200 °C is indicative of the fact that the amount of SiO₂ in the protective film is insufficient for covering the total surface of the composites quickly, as a result of which further oxidation takes

place. The protective film with a higher amount of SiO_2 has indeed been found to form at 1300°C . The improved oxidation resistance of the ZSS compared to that of the ZS is attributed to the former composite's Si_3N_4 content, which enhances both the amount and the rate of SiO_2 formation along with that of $\text{Si}_2\text{N}_2\text{O}$, thereby making the oxide scale more protective. This suggests that the presence of Si_3N_4 in addition to SiC is beneficial for improving the oxidation resistance of the ZrB_2 -based composite.

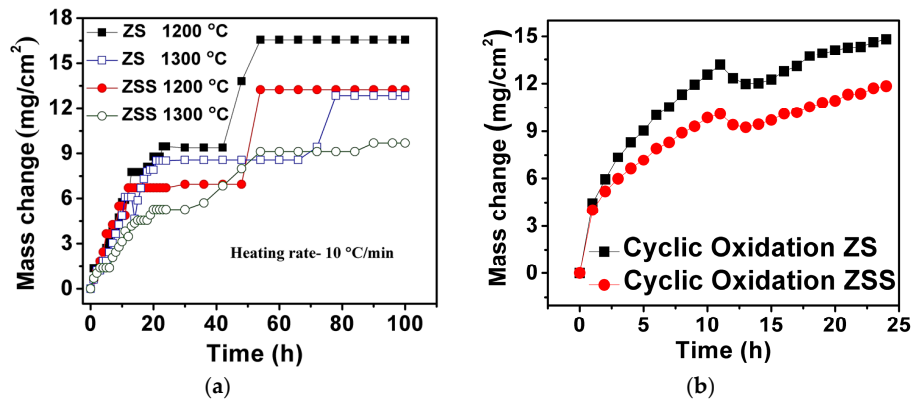


Figure 2. Plots of change in mass against time obtained from (a) isothermal; and (b) cyclic oxidation tests carried out on ZS and ZSS for duration of 100 h at 1200 and 1300°C .

The oxide scale constituents have been examined in order to understand the probable oxidation mechanisms. XRD patterns of the oxide scales formed at 1300°C for 24 h on the investigated composites are depicted in Figure 3. The results in this figure indicate that (i) the peaks representing monoclinic and tetragonal ZrO_2 as well as those of ZrSiO_4 are present in all the XRD patterns, while (ii) the peaks of $\text{Si}_2\text{N}_2\text{O}$ are present only in the XRD pattern of the oxide scale formed on the ZSS composite.

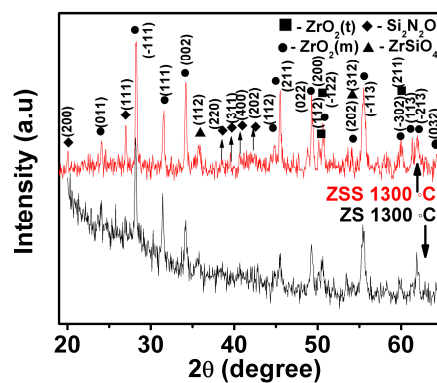


Figure 3. XRD patterns obtained from the oxide scales formed on the ZS and ZSS composites after isothermal oxidation at 1300°C for 100 h in air. Comparison of peak intensities reveals that ZrO_2 (m) is the major constituent, whereas ZrO_2 (t) and ZrSiO_4 are the minor constituents of the oxide scales. Evidence of $\text{Si}_2\text{N}_2\text{O}$ peaks is noted for the ZSS composite.

Figure 4 shows typical SEM images depicting the oxide scale surfaces formed on ZS and ZSS composites. These results show that the oxide scale formed on the ZSS has a greater amount of continuity than that formed on the ZS. Microcracks are visible on both these oxide scales and the area-fraction of microcracks is higher on the oxide scale formed on the ZS. Using EDS analysis, the products of oxidation have been found to be a mixture of ZrO_2 and SiO_2 ; but the absence of SiO_2 peaks in the XRD patterns is attributed to its amorphous character. The presence of $\text{Si}_2\text{N}_2\text{O}$ in oxide scale of ZSS is further confirmed by EDS analysis showing peaks of Si, N and O in the spectrum (Figure 4h (inset)).

A set of EPMA (BSE) images depicting cross-sections of the oxide scale formed on the ZSS after exposure at 1200 °C for 100 h are shown in Figure 5. When ZS and ZSS are isothermally held at 1200 and 1300 °C, the oxidation products consist of (i) a layer of SiO₂, followed by (ii) a layer of ZrO₂-SiC. The compositions of these layers have been confirmed by EDS mapping, while the thickness values of the individual layers of the oxide scales formed on ZS and ZSS at 1200 or 1300 °C for 24 or 100 h have been assessed by analyzing different SEM and EPMA images of the cross-sections and the oxide scale thicknesses are shown in Figure 5e. Comparison of the results in this figure shows that the thickness of the oxide scale formed on the ZSS is much less than that on ZS, and the difference is more significant at 1200 °C than that at 1300 °C.

The main reactions involved during oxidation of ZS and ZSS composites at 1200 and 1300 °C are:

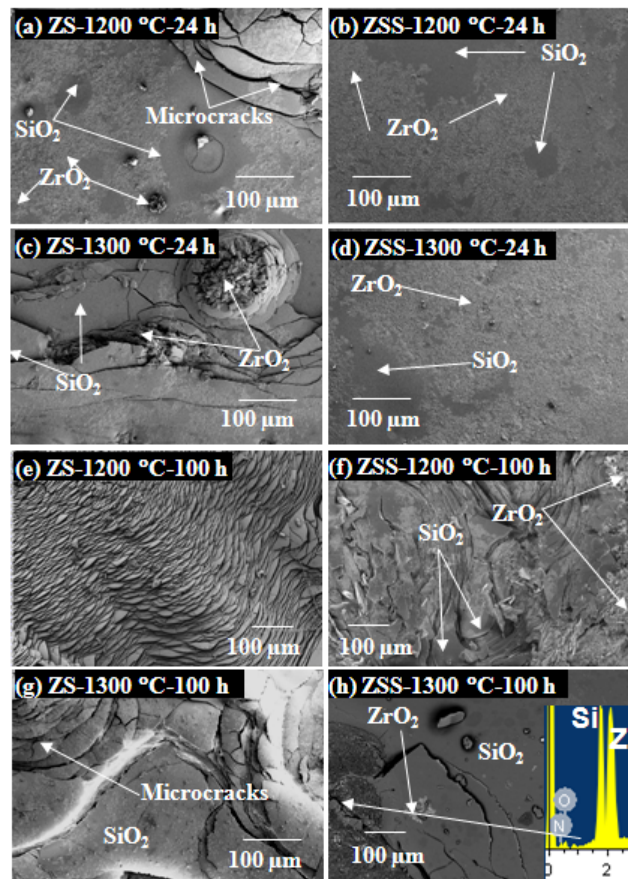
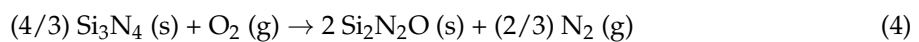
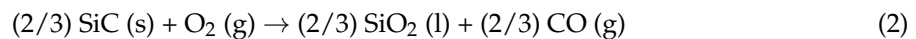
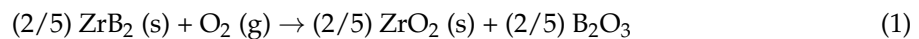


Figure 4. SEM micrographs depicting morphology of the surfaces of the oxide scales formed by isothermal oxidation in air on: (a) ZS at 1200 °C for 24 h; (b) ZSS at 1200 °C for 24 h; (c) ZS at 1300 °C for 24 h; (d) ZSS at 1300 °C for 24 h; (e) ZS at 1200 °C for 100 h; (f) ZSS at 1200 °C for 100 h; (g) ZS at 1300 °C for 100 h; and (h) ZSS at 1300 °C for 100 h. Oxide products are mainly composed of ZrO₂ and silica rich glassy phases. Several micro-cracks are observed on the oxide surfaces. The density of micro-cracks is more on ZS composite, whereas the amount of silica reaching the glassy layer is higher on ZSS composite.

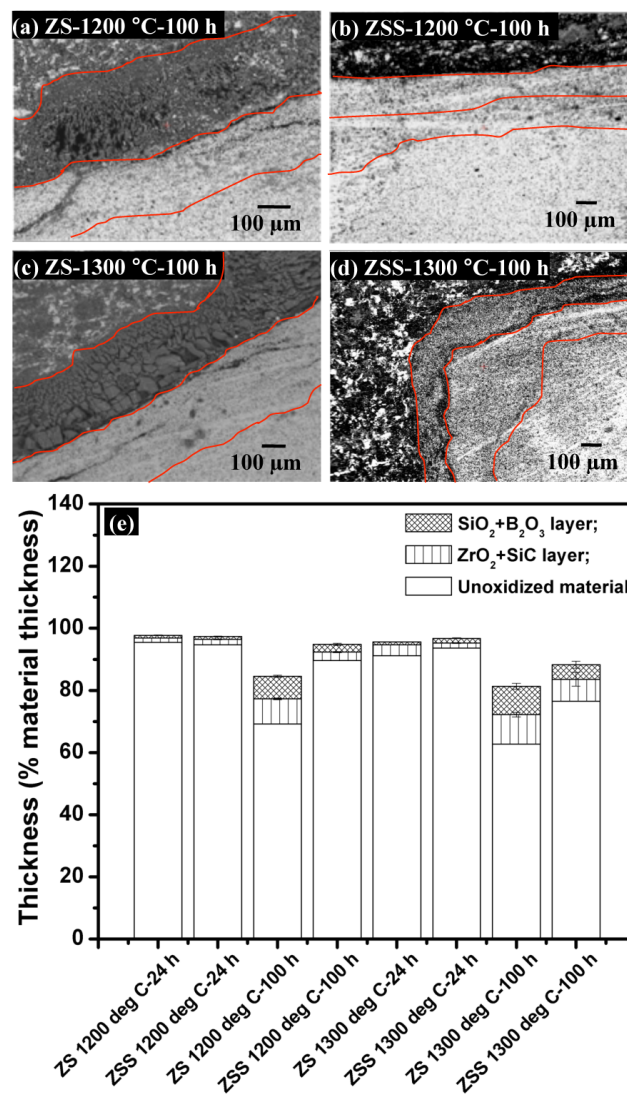


Figure 5. Cross-sections of oxides scale formed by isothermal oxidation for 100 h in air: (a) ZS at 1200 °C; (b) ZSS at 1200 °C; (c) ZS at 1300 °C; and (d) ZSS at 1300 °C. The oxide scales exhibit a layer of SiO₂-B₂O₃ followed by a layer of ZrO₂-SiC; (e) Thicknesses of unoxidized part of specimens, and the layers within the oxide scales formed on ZS and ZSS, subjected to exposure at 1200 or 1300 °C for 24 or 100 h.

The dominant chemical reactions operative during oxidation of ZS and ZSS between 1200 and 1300 °C are: oxidation of ZrB₂ by reaction (1); oxidation of SiC by reaction (2); and evaporation of B₂O₃ [3] by reaction (3). Vaporization of B₂O₃ leaves behind porous ZrO₂, which gets subsequently filled by SiO₂, formed by oxidation of SiC. On the other hand, Si₃N₄ preferably first oxidizes according to reaction (4). The ZSS shows lower mass gain compared to other ZrB₂-based composites during oxidation at both 1200 and 1300 °C due to the presence of Si₃N₄. The oxidation of Si₃N₄ results in the formation of duplex oxidation scale consisting of SiO₂ and Si₂N₂O phase. The Si₂N₂O appears to have formed as an intermediate phase between SiO₂ and Si₃N₄ in the range of 1200–1400 °C. It has been shown that Si₂N₂O provides a stronger diffusion barrier for O₂ better compared to SiO₂ [15]. However, the SiO₂ is more thermodynamically stable than Si₂N₂O at the investigated temperature regimes. The Gibbs free energy of formation ΔG_f° is lower for amorphous SiO₂ ($\Delta G_f^\circ = -154.6$ kJ/mol at 1200 °C) than for Si₂N₂O ($G_f^\circ = -127.5$ kJ/mol at 1200 °C) [16].

The beneficial effect of SiC and Si₃N₄ addition towards oxidation resistance of ZS and ZSS at the selected temperature regimes is due to the formation of borosilicate glass layer. A part of B₂O₃

vaporizes while the remaining part reacts with SiO_2 to form the borosilicate glass; the presence of B on the oxidized surface has been confirmed by EPMA analysis. The SiO_2 rich layer however provides an effective barrier to oxygen diffusion and leads to passive oxidation protection at 1200 and 1300 °C [2,17]. It is clear that the gain in mass occurs due to the formation of ZrO_2 and SiO_2 , while the mass loss can be attributed to the escape of B_2O_3 (g) and CO (g).

Higher degradation of the oxide scales of both ZS and ZSS in cyclic compared to isothermal oxidation tests is evident from the images depicted in Figures 3 and 6. This degradation in terms of cracking and spallation can be attributed to (i) the CTE mismatch between the oxide scale constituents and substrate; and (ii) the volume change associated with phase transformation of t- ZrO_2 to m- ZrO_2 in the oxide scale. The CTE values of amorphous SiO_2 ($\alpha = 0.5 \times 10^{-6}/^\circ\text{C}$) and crystalline $\text{Si}_2\text{N}_2\text{O}$ ($\alpha = 2.86 \times 10^{-6}/^\circ\text{C}$) [18] are considerably lower than that of ZrB_2 ($\alpha = 5.9 \times 10^{-6}/^\circ\text{C}$) or m- ZrO_2 ($\alpha = 7 \times 10^{-6}/^\circ\text{C}$). The residual stress, σ developed by CTE mismatch in a phase after one thermal cycle can be estimated as:

$$\sigma = [E/(1 - \nu)] \cdot [\Delta\alpha \times \Delta T] \quad (5)$$

where E is the Young's modulus, ν is the Poisson's ratio, $\Delta\alpha$ is the CTE mismatch and ΔT is the temperature difference. The magnitudes of σ due to the CTE mismatch between the constituent phases, $\text{ZrO}_2/\text{SiO}_2$, $\text{ZrO}_2/\text{Si}_2\text{N}_2\text{O}$ and $\text{ZrO}_2/\text{ZrB}_2$ systems during heating are 1700, 1082 and 287 MPa, respectively. Hence, presence of $\text{Si}_2\text{N}_2\text{O}$ in the oxide scale would reduce its tendency for cracking or spallation. This is considered as the primary reason for lower degradation of ZSS as compared to ZS. The principal residual stresses, σ_1 and σ_3 , as well as the maximum shear stress, $\tau_{\text{max}} [= (\sigma_1 - \sigma_2)/2]$ within m- ZrO_2 phase present in the oxide scales of ZSS are 216, 381 and -82 MPa, respectively. The magnitudes of the experimentally estimated residual stress values are considerably lower compared to calculated values based on CTE mismatch. The stress relief caused by cracking during exposure to multiple thermal cycles appears to be the most acceptable explanation for the differences between calculated (for single cycle) and experimental (multiple cycles) values of residual stress, as shown in Table 2.

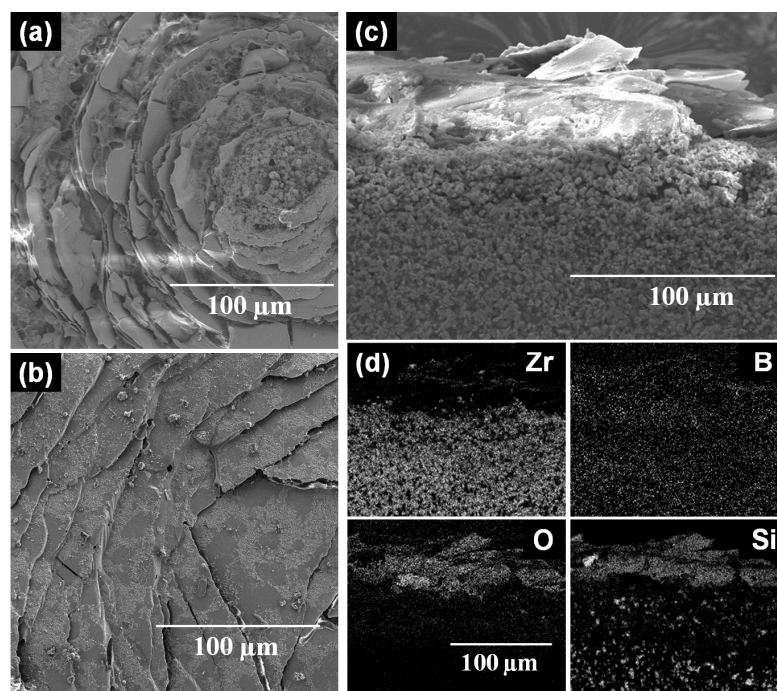


Figure 6. SEM micrographs depicting the top surface of oxide scale formed by cyclic oxidation for 24 h in air at 1300 °C on: (a) ZS, (b) ZSS and Cross-section of the oxide scale formed on ZSS; (c) SEM (BSE) image, as well as (d) EDS maps of Zr, B, O, and Si.

4. Summary

Mass change and evolution of microstructures in the oxide scales produced by exposure of hot pressed ZrB₂-20 vol % SiC (ZS) as well as ZrB₂-20 vol % SiC-5 vol % Si₃N₄ (ZSS) have been studied in air at 1200 and 1300 °C for 24 and 100 h. The results of oxidation studies reveal that the ZSS undergoes lower change in mass than the ZS on being exposed to both isothermal and cyclic exposures at both 1200 and 1300 °C. Furthermore, the mass gain under cyclic exposure conditions are found to be significantly higher than those under isothermal conditions. Oxidation of both SiC and Si₃N₄ in the ZSS results in the formation of a duplex oxide scale consisting of SiO₂ and Si₂N₂O phases. The formation of Si₂N₂O phase in the oxide scale of the ZSS has been confirmed by XRD analysis, and is well supported by thermodynamic calculations. The formation of excess silica-rich phase in the ZSS compared to that in the ZS helps in closure of pores, and reduces the possibility of crack generation. As a result, the diffusion barrier for oxygen anions in the oxide scale of the ZSS is strengthened, and this results in greater oxidation resistance.

Acknowledgments: The financial support from Defence Research and Development Organization, New Delhi is gratefully acknowledged. The authors also express their sincere gratitude to technical personnel at the Central Research Facility, Indian Institute of Technology, Kharagpur, West Bengal, India.

Author Contributions: The present work has been carried out as a part of the Ph.D. dissertation research by Manab Mallik under the guidance of Kalyan Kumar Ray and Rahul Mitra as his advisors. Kalyan Kumar Ray and Rahul Mitra have contributed in planning the work, interpretation and explanation of the results as well as preparation of this manuscript.

Conflicts of Interest: The authors declare no conflict of interest.

References

1. Cutler, R.A. *Engineered Materials Handbook, Ceramics and Glasses*; ASM International: Metals Park, OH, USA, 1991; Volume 4, pp. 787–803.
2. Opeka, M.M.; Talmy, I.G.; Wuchina, E.J.; Zaykoski, J.A.; Causey, S.J. Mechanical, Thermal, and Oxidation Properties of Refractory Hafnium and Zirconium Compounds. *J. Eur. Ceram. Soc.* **1999**, *19*, 2405–2414. [[CrossRef](#)]
3. Talmy, I.G.; Zaykoski, J.A.; Opeka, M.M. High-Temperature Chemistry and Oxidation of ZrB₂ Ceramics Containing SiC, Si₃N₄, Ta₅Si₃ and TaSi₂. *J. Am. Ceram. Soc.* **2008**, *91*, 2250–2257. [[CrossRef](#)]
4. Sciti, D.; Brach, M.; Bellosi, A. Long-term oxidation behavior and mechanical strength degradation of a pressurelessly sintered ZrB₂-MoSi₂ ceramic. *Scr. Mater.* **2005**, *53*, 1297–1302. [[CrossRef](#)]
5. Bellosi, A.; Montevede, F. Ultra-Refractory Ceramics: The Use of Sintering Aids to Obtain Microstructural Control and Properties Improvement. *Key Eng. Mater.* **2003**, *264–268*, 787–792. [[CrossRef](#)]
6. Mallik, M.; Ray, K.K.; Mitra, R. Oxidation behavior of hot pressed ZrB₂-SiC and HfB₂-SiC composites. *J. Eur. Ceram. Soc.* **2011**, *31*, 199–215. [[CrossRef](#)]
7. Fahrenholtz, W.G.; Hilmas, G.E.; Chamberlain, A.L.; Zimmermann, J.W. Processing and characterization of ZrB₂-based ultra-high temperature monolithic and fibrous monolithic ceramics. *J. Mater. Sci.* **2004**, *39*, 5951–5957. [[CrossRef](#)]
8. Monteverde, F.; Bellosi, A. Effect of the addition of silicon nitride on sintering behaviour and microstructure of zirconium diboride. *Scr. Mater.* **2002**, *46*, 23–28. [[CrossRef](#)]
9. Mallik, M.; Kailath, A.J.; Ray, K.K.; Mitra, R. Electrical and thermophysical properties of ZrB₂ and HfB₂ based composites. *J. Eur. Ceram. Soc.* **2012**, *32*, 2545–2555. [[CrossRef](#)]
10. Cullity, B.D. *Elements of X-ray Diffraction*; Addison Wesley Publishing Company, Inc.: New York, NY, USA, 1978; pp. 447–478.
11. Schumann, E.; Sarioglu, C.; Blachere, J.R.; Pettit, F.S.; Meier, G.H. High temperature stress measurements during the oxidation of NiAl. *Oxid. Met.* **2000**, *53*, 259–272. [[CrossRef](#)]
12. Paswan, S.; Mitra, R.; Roy, S.K. Oxidation behavior of Mo-Si-Band Mo-Si-B-Al alloys. *Metall. Mater. Trans. A* **2009**, *40*, 2644–2658. [[CrossRef](#)]

13. Mitra, R.; Upender, S.; Mallik, M.; Chakraborty, S.; Ray, K.K. Mechanical, thermal, and oxidation behaviour of zirconium diboride based ultra-high temperature ceramic composites. *Key Eng. Mater.* **2009**, *395*, 55–68. [[CrossRef](#)]
14. Monteverde, F.; Bellosi, A. Oxidation of ZrB₂-Based Ceramics in Dry Air. *J. Electrochem. Soc.* **2003**, *150*, B552–B559. [[CrossRef](#)]
15. Fordham, R.J. *High Temperature Corrosion of Technical Ceramics*; Elsevier Applied Science: New York, NY, USA, 1990.
16. Taguchi, S.P.; Ribeiro, S. Silicon nitride oxidation behaviour at 1000 °C and 1200 °C. *J. Mater. Process. Technol.* **2004**, *147*, 336–342. [[CrossRef](#)]
17. Levine, S.R.; Opila, E.J.; Halbig, M.C.; Kiser, J.D.; Singh, M.; Salem, J.A. Evaluation of ultra high temperature ceramics for aer propulsion use. *J. Eur. Ceram. Soc.* **2002**, *22*, 2757–2767. [[CrossRef](#)]
18. Billy, M.; Boch, P.; Dumazeau, C.; Glandus, J.C.; Goursat, P. Preparation and properties of new silicon oxynitride based ceramics. *Ceram. Int.* **1981**, *7*, 13–18. [[CrossRef](#)]



© 2017 by the authors. Licensee MDPI, Basel, Switzerland. This article is an open access article distributed under the terms and conditions of the Creative Commons Attribution (CC BY) license (<http://creativecommons.org/licenses/by/4.0/>).